Article

Optimization of the Synthesis of SAPO-11 for the Methylation of Naphthalene with Methanol by Varying Templates and Template Content

Xiaoxiao Wang,[a,b] Wei Zhang,[,a] Shaoqing Guo,[c] Liangfu Zhao[*,a] and Hongwei Xiang[a]*

[a]*Institute of Coal Chemistry, Chinese Academy of Sciences, Taiyuan 030001,
People's Republic of China*

[b]*University of Chinese Academy of Sciences, Beijing 100049, People's Republic of China*

[c]*Taiyuan University of Science and Technology, Taiyuan 030024, People's Republic of China*

Zeólitas SAPO-11 foram sintetizadas com sucesso utilizando três diferentes direcionadores orgânicos (dietilamina (DEA), di-*n*-propilamina (DPA) e di-isopropilamina (DIPA)) e um conteúdo variável de DPA (nDPA/Al$_2$O$_3$ = 0,8, 1,2, 1,6 e 2,0) sob condições hidrotérmicas. As amostras foram caracterizadas por difratometria de raios X de pó (XRD), microscopia eletrônica de varredura (SEM), adsorção-desorção de N$_2$, dessorção de amônia a temperatura programada (NH$_3$-TPD) e ressonância magnética nuclear (NMR) de ^{29}Si com rotação no ângulo mágico (MAS). As amostras foram também avaliadas com relação à metilação do naftaleno com metanol para obtenção de 2,6-dimetil-naftaleno (2,6-DMN). Resultados de difratometria de raios X indicaram que o efeito direcional das diferentes aminas sobre a estrutura AEL (Aluminophosphate-ELeven) decresceram segundo a ordem DPA > DEA > DIPA e o conteúdo de DPA mais adequado foi nDPA/Al$_2$O$_3$ = 1,2. Resultados da adsorção-desorção de N$_2$ mostraram que SAPO-11(DPA,1.2) exibiu a distribuição de poros mais ampla, a área superficial específica BET mais elevada e o volume de poro maior dentre todas as amostras SAPO-11. SAPO-11(DPA,1.2) exibiu também um elevado desempenho catalítico na metilação de naftaleno devido às suas elevadas cristalinidade e superfície externa e à ampla distribuição de tamanho de poro. A estrutura de poros da zeólita SAPO-11, ao invés de sua acidez, desempenhou um papel importante na obtenção de elevado desempenho catalítico na metilação de naftaleno com metanol.

SAPO-11 zeolites were successfully synthesized by using three different templates (diethylamine (DEA), di-*n*-propylamine (DPA) and di-isopropylamine (DIPA)) and varying DPA contents (nDPA/Al$_2$O$_3$ = 0.8, 1.2, 1.6 and 2.0) under hydrothermal conditions. The samples were characterized by powder X-ray diffractometry (XRD), scanning electron microscopy (SEM), N$_2$ adsorption-desorption, temperature programmed desorption of ammonia (NH$_3$-TPD) and ^{29}Si magic angle spinning (MAS) nuclear magnetic resonance (NMR). The samples were also evaluated towards the methylation of naphthalene with methanol to produce 2,6-dimethylnaphthalene (2,6-DMN). XRD results indicated that the directing effect of the different templates for AEL (Aluminophosphate-ELeven) structure decreased in the order DPA > DEA > DIPA and the most suitable DPA content was nDPA/Al$_2$O$_3$ = 1.2. N$_2$ adsorption-desorption results showed that SAPO-11(DPA,1.2) exhibited the broadest pore size distribution, the highest BET specific surface area and the largest pore volume among all the SAPO-11 samples. SAPO-11(DPA,1.2) exhibited high catalytic performances in the methylation of naphthalene due to its high crystallinity, high external surface and broad pore size distribution. The pore structure of SAPO-11 zeolite, rather than its acidity, played an important role in achieving high catalytic performances in the methylation of naphthalene with methanol.

Keywords: SAPO-11, templates, template content, methylation of naphthalene

*e-mail: zw7234@sxicc.ac.cn, lfzhao@sxicc.ac.cn

Introduction

2,6-Dimethylnaphthalene (2,6-DMN) is a preferred monomer for high-performance polymeric materials. The synthesis of 2,6-DMN by methylation of naphthalene with methanol over zeolites has aroused much attention due to its simple synthetic route and low production cost. Some zeolites have been studied for the methylation of naphthalene, such as ZSM-5, HY, ZSM-12 and Beta.[1-4] However, they did not show both high naphthalene conversion and high 2,6-DMN yield in the methylation of naphthalene.

The SAPO-11 zeolite is a member of the silico-aluminophosphate (SAPO-n) family which was first synthesized by Union Carbide Corporation.[5] It has novel pore structures and exhibits milder acidity due to the presence of phosphorus.[6] It is a one-dimensional pore zeolite with a pore size of 0.39×0.64 nm, which has shown catalytic performances in alkylation reactions such as alkylation of toluene, alkylation of biphenyl and methylation of aniline.[7-9] The pore size of SAPO-11 is larger than 0.60 nm, which can effectively sieve the products of naphthalene methylation.[1] Also, its high catalytic performance has been proved in the methylation of naphthalene in our previous work.[10,11]

It has been reported that the template played an important role in the synthesis of SAPO-11 zeolite for achieving a given structure or stabilizing certain phases. One template may produce SAPO-11 with different structures by varying synthetic conditions, and one type of SAPO-11 could also be synthesized in the presence of different templates. Similarly, different template contents play important roles in the synthesis of SAPO-11 (structure-directing, space filling and charge compensation roles). The physicochemical properties of SAPO-11 may also change with different templates and different template contents. In consequence, the catalytic performance of SAPO-11 could be different. The studies about the influence of template or template content on the catalytic performances of SAPO-11 have not been reported in the methylation of naphthalene so far. In this work, in order to investigate the influence of template and template content on the physicochemical and catalytic performances of SAPO-11 in the methylation of naphthalene, a set of SAPO-11 zeolites was synthesized with different templates and different template contents by hydrothermal method. The physicochemical properties of SAPO-11 samples were characterized by XRD (X-ray powder diffractometry), SEM (scanning electron microscopy), N_2 adsorption-desorption, NH_3-TPD (temperature programmed desorption of ammonia) and ^{29}Si magic angle spinning (MAS) nuclear magnetic resonance (NMR), and their catalytic performances were also studied for the methylation of naphthalene with methanol.

Experimental

Catalyst preparation

SAPO-11 was synthesized hydrothermally with a composition of $1.0Al_2O_3:1.0P_2O_5:0.6SiO_2:1.2R:49H_2O$, where R represented the template. Pseudoboehmite, orthophosphoric acid and silica sol were used as source of Al, P and Si, respectively. Diethylamine (DEA), di-*n*-propylamine (DPA) and di-isopropylamine (DIPA) were used in the synthesis to investigate the influence of the template on the catalytic properties of SAPO-11. The final crystallization temperature of 200 ºC and crystallization time of 24 h were employed. The as-synthesized samples were washed with distilled water, then dried at 120 ºC for 12 h and calcined at 600 ºC for 4 h. The samples were prepared from different templates and with a molar ratio of template (DEA, DPA, DIPA) to Al_2O_3 of 1.2; thus the samples synthesized were denoted as SAPO-11(DEA,1.2), SAPO-11(DPA,1.2) and SAPO-11(DIPA,1.2), respectively.

SAPO-11 was also synthesized with different DPA template contents for comparison. The gel molar composition was $1.0Al_2O_3:1.0P_2O_5:0.6SiO_2:xDPA:49H_2O$, where x is the molar ratio of DPA to Al_2O_3 and equals 0.8, 1.2, 1.6 and 2.0, respectively. All the raw materials and synthesis process were the same as above. The samples prepared with template contents of 0.8, 1.2, 1.6 and 2.0 were denoted as SAPO-11(DPA,0.8), SAPO-11(DPA,1.2), SAPO-11(DPA,1.6) and SAPO-11(DPA,2.0), respectively.

Catalyst characterization

XRD analysis was performed on RigakuD/maxrB X-ray diffractometer. Diffraction patterns were recorded with Cu K_α radiation at 40 kV and 100 mA in the scan range between 5º and 50º to identify the phase structure of the samples.

The textural properties of the samples were derived from N_2 adsorption-desorption measurement on Micromeritics Tristar 3000. In each case, the sample was outgassed under vacuum at 300 ºC for 3 h before N_2 adsorption. The specific surface area was calculated according to the BET method and the pore volume was obtained by t-plot analysis of the adsorption isotherm.

SEM analysis was performed with a LEO-435VP scanning electron microscope operated at 20 kV and 50 pA.

The acidity was examined by temperature programmed desorption of ammonia (NH_3-TPD). NH_3-TPD was carried out in a flow system with a thermal conductivity detector.

All samples were preheated from room temperature to 500 °C in argon flow and kept at 500 °C for 1 h, which was followed by NH_3 saturation in a flowing NH_3/Ar stream at 40 °C for 5 min. Evacuation at 40 °C for 40 min was carried out to remove physically adsorbed NH_3. Finally, the sample was heated to 600 °C at a linear heating rate of 10 °C min^{-1}, and the detector signal of NH_3 was recorded.

^{29}Si MAS NMR experiments were recorded on Varian Infinity Plus-300 NMR equipment. All ^{29}Si MAS NMR spectra were recorded at 79.5 MHz using 2.0 μs pulse with 3.0 recycle delay and 7120 scans.

Catalyst evaluation

The experiments were performed in a fixed-bed continuous-flow reactor equipped with a 20 mm diameter and 600 mm length stainless steel tube. 2.5 g of 20-40 mesh zeolite catalysts were loaded in the reaction tube. The reaction mixture was fed into the reactor by a quantity measuring pump and the pressure was kept with N_2. The weight hourly space velocity (WHSV) of naphthalene was 0.19 h^{-1} in all experiments. The reaction temperature was 400 °C and the liquid reactant including naphthalene, methanol and mesitylene (solvent) in a molar ratio of 1:5:3.5 was preheated before passing to the reactor. Reaction products were analyzed by gas chromatography (GC9560) with a Beta-Dex120 capillary column. The naphthalene conversion was calculated as follows:

$$\text{Naphthalene conversion (mol\%)} = \frac{n_{N,0} - n_N}{n_{N,0}} 100 \qquad (1)$$

where $n_{N,0}$ and n_N are the molar percentages of naphthalene before and after the reaction, respectively. 2,6-/2,7-DMN stands for the molar ratio of 2,6-DMN to 2,7-DMN.

$$\text{2,6-DMN yield} = \frac{\text{naphthalene conversion} \times \text{2,6-DMN distribution}}{100\%} \qquad (2)$$

Results and Discussion

Physicochemical properties

Figure 1 shows the XRD patterns of as-synthesized SAPO-11 samples. As seen in Figure 1a, the directing effect of different templates for Aluminophosphate-ELeven (AEL) structure decreases in the order DPA > DEA > DIPA. SAPO-11(DIPA,1.2) has an extra peak at 7.4°, indicating the presence of the SAPO-5 phase. Figure 1b exhibits the XRD patterns of SAPO-11 samples with different DPA contents. As shown in Figure 1b, the sample called SAPO-11(DPA,0.8) is not a true SAPO-11 phase and the

material can be identified to be tridymite, which is probably produced due to the deficiency of template. When the template content increases to 2.0, the synthesized sample is an amorphous material. It is caused possibly by the high template amount, which leads to a high pH value of the starting gel and further hinders the nucleation of SAPO-11.[12-13] As seen in Figure 1, the SAPO-11 sample shows the highest crystallinity when DPA is used as the template and nDPA/Al_2O_3 = 1.2, followed by SAPO-11(DPA,1.6), then SAPO-11(DEA,1.2).
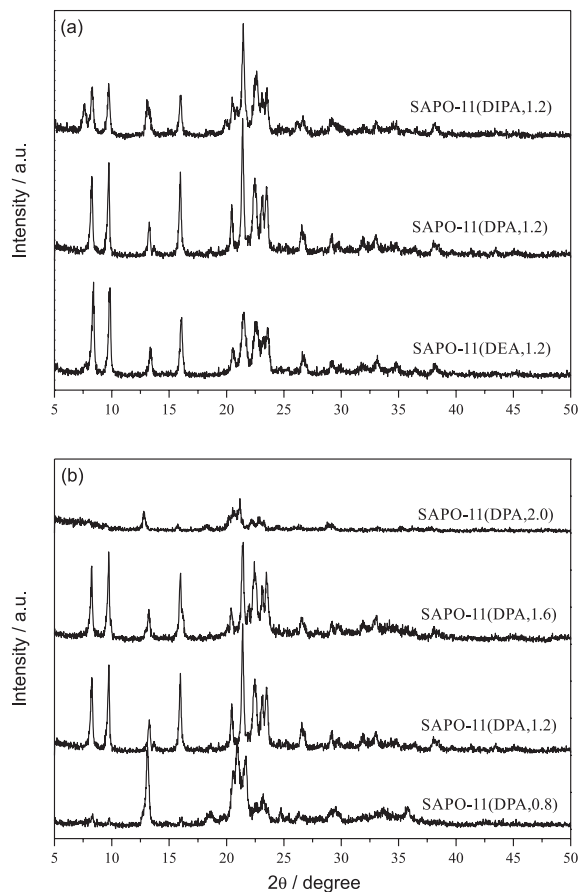

Figure 1. XRD patterns of SAPO-11 samples. (a) XRD patterns of SAPO-11 samples synthesized with different templates; and (b) XRD patterns of SAPO-11 samples synthesized with different DPA contents.

SEM micrographs of SAPO-11(DEA,1.2), SAPO-11(DPA,1.2) and SAPO-11(DPA,1.6) are presented in Figure 2. SAPO-11(DEA,1.2) shows an irregular surface morphology, consisting of spherical particles with the average crystal size of about 20 μm. SAPO-11(DPA,1.2) and SAPO-11(DPA,1.6) present homogeneous spherical particles. The average crystal size of SAPO-11(DPA,1.2) and SAPO-11(DPA,1.6) is more than 20 μm and the former is larger than the latter. According to the literature,[14] zeolites with high crystallinity show a regular morphology. SAPO-11(DPA,1.2) shows a more

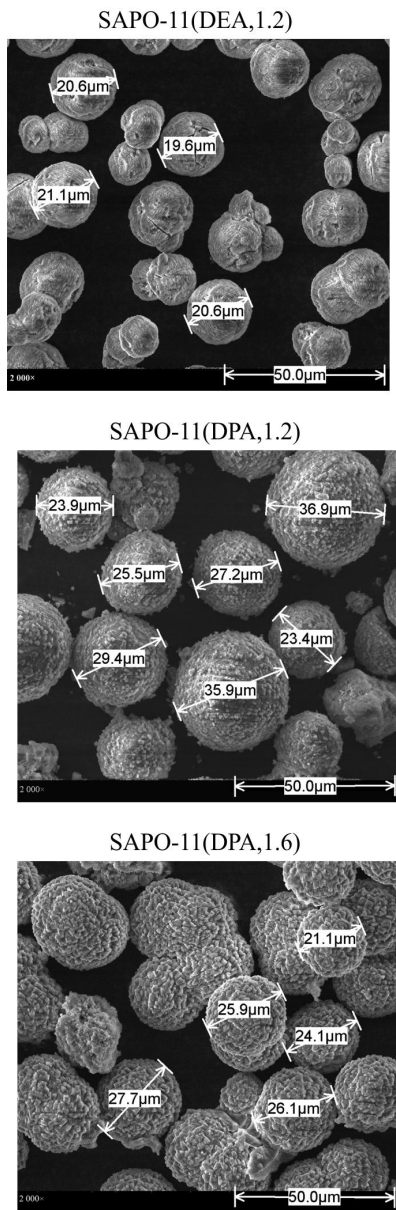SAPO-11(DEA,1.2)

SAPO-11(DPA,1.2)

SAPO-11(DPA,1.6)

Figure 2. SEM profiles of as-synthesized SAPO-11 samples.

regular morphology than that of SAPO-11(DEA,1.2) and SAPO-11 (DPA,1.6), in agreement with results of the XRD analysis (Figure 1).

The N_2 adsorption-desorption isotherms of as-synthesized SAPO-11 samples are shown in Figure 3. The typical N_2 adsorption-desorption isotherms of the SAPO-11 samples are of the type IV according to the IUPAC classification. High adsorption of N_2 occurred in the low relative pressure range and obvious hysteresis was detected for the samples, suggesting the existence of micropores and mesopores in the as-synthesized SAPO-11 samples, fully demonstrated in Figure 4. Figure 4 shows micropores and secondary mesopore size distributions of the SAPO-11 samples. In general, the secondary mesopores probably result from

SAPO-11 microcrystals piled up in the synthesis process. As seen in Figure 4, SAPO-11(DPA,1.2) has broader micropore size distributions and secondary mesopore size distributions compared with the other SAPO-11 samples. Also, the pore structure parameters of the samples (see Table 1) show that SAPO-11(DPA,1.2) possesses higher specific surface area and larger pore volume than the other two SAPO-11 samples, which corresponds to the higher crystallinity of SAPO-11(DPA,1.2).[15]
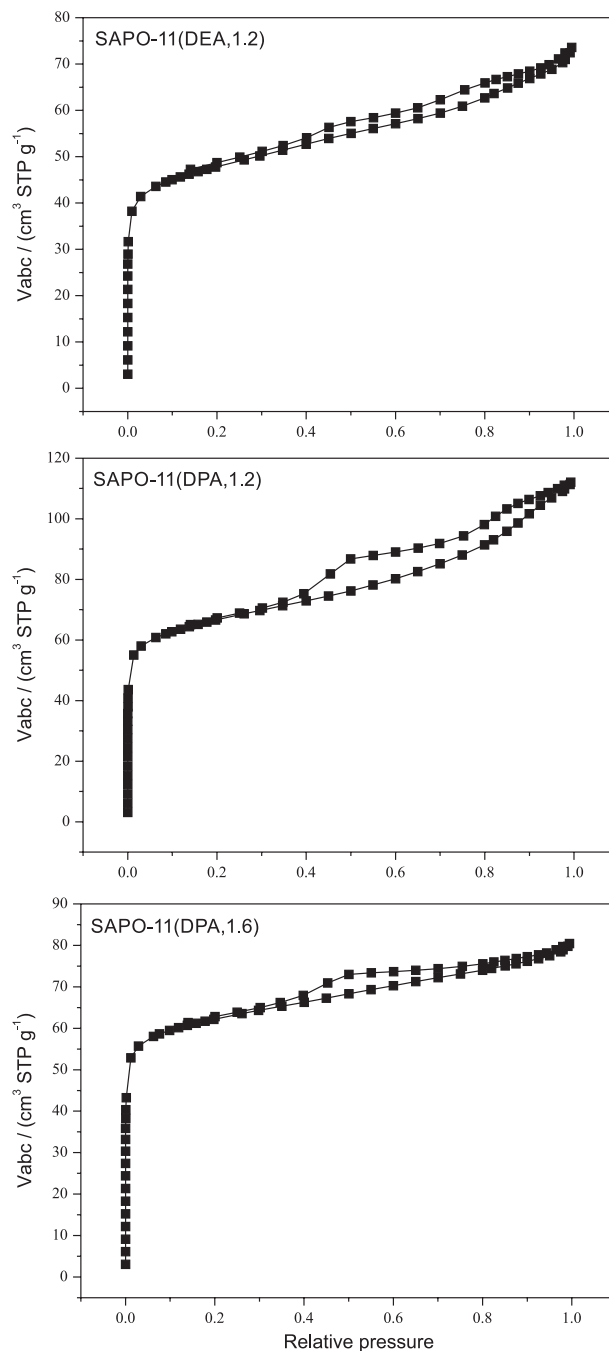

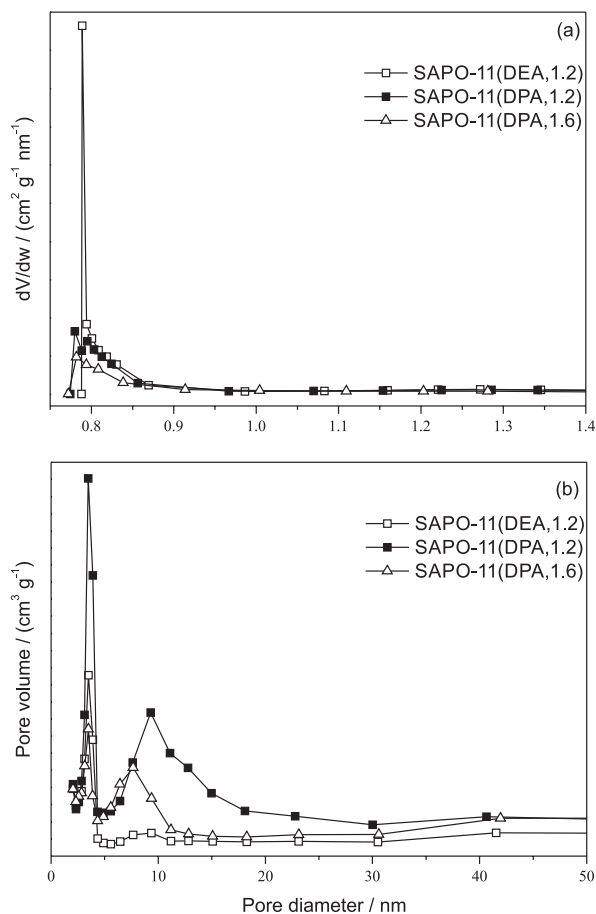**Figure 3.** N_2 adsorption-desorption isotherms of as-synthesized SAPO-11 samples.

Figure 4. Pore size distributions of as-synthesized SAPO-11 samples: (a) micropore size distributions, and (b) secondary mesopore size distributions.

The acid amount and the acid strength of several zeolites were determined by NH_3-TPD. The NH_3-TPD profiles are presented in Figure 5. The acid amount is estimated from the areas underlying the TPD curves and the acid strength is characterized by the ammonia desorption peak temperature. Meanwhile, the values of acidity of the SAPO-11 samples are shown in Table 2. As seen from Figure 5 and Table 2, the acidity of SAPO-11(DPA,1.2) and SAPO-11(DPA,1.6) are much the same. However, SAPO-11(DEA,1.2) has less acid sites than SAPO-11(DPA,1.2) and SAPO-11(DPA,1.6), in both the amount of total acid sites and the amount of medium strength acid sites, which probably results from

their great difference in crystallinity. Certainly, the different Si distribution over these samples must be taken into account. It is reported that the acidic properties of SAPO-11 depend on the way in which the Si atoms are incorporated into the framework.[16-17] Generally, the substitution of a Si atom by an Al atom (SM1) could not occur due to the formation of undesirable Si−O−P linkages. The substitution of a Si atom by a P atom (SM2) produced an isolated Si (4Al) site, giving rise to acid sites with weak strength. SM3 mechanism involves the substitution of an Al−O−P pair by two Si atoms combined with the substitution of the three P atoms adjacent to the aluminum by three more Si, to avoid the formation of Si−O−P linkages. Such substitution forms silica islands and produces Si (n Al, 4-n Si, 0 < n < 4) environments. The inside Si atoms in Si islands hardly generate the acidity, and the acid sites with medium strength could be produced from the border of silicon domains. In general, SM2 gives rise to more acid sites than SM3 does at the same silicon content, and it is independent of the acid strength.
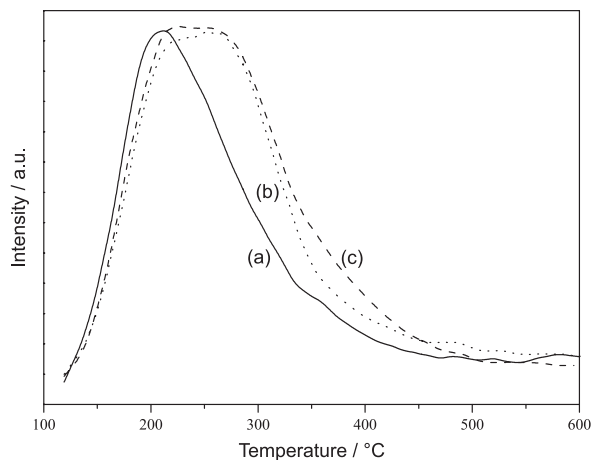

Figure 5. NH_3-TPD profiles of SAPO-11 samples: (a) SAPO-11(DEA,1.2), (b) SAPO-11(DPA,1.2) and (c) SAPO-11(DPA,1.6).

^{29}Si MAS NMR experiments were performed to investigate the local environments of the Si atoms incorporated into the framework (Figure 6). Figure 6 shows that the spectrum of SAPO-11(DEA,1.2) is dominated by the low-field signal (between *ca.* −110 and *ca.* −100 ppm)

Table 1. Pore structure parameters of as-synthesized SAPO-11 samples

Sample	Specific surface area / ($m^2 g^{-1}$)			Pore volume / ($cm^3 g^{-1}$)			Average pore diameter	
	BET[a]	Micropore[b]	External	Total[c]	Micrpore[b]	Mesopore	Mesopore[a]	Micropore[d]
SAPO-11(DEA,1.2)	166	101	65	0.113	0.047	0.066	2.352	0.827
SAPO-11(DPA,1.2)	228	145	83	0.173	0.067	0.106	3.040	0.853
SAPO-11(DPA,1.6)	211	138	73	0.141	0.048	0.093	2.782	0.835

[a]BET method; [b]t-plot method; [c]volume adsorbed at $P/P_0 = 0.99$; [d]Horvath-Kawazoe method.

Table 2. Acidity values of as-synthesized SAPO-11 samples

Sample	Weak acid site		Medium strong acid site		The total acid amount / (mmol g⁻¹)
	Peak temperature / °C	Acid amount / (mmol g⁻¹)	Peak temperature / °C	Acid amount / (mmol g⁻¹)	
SAPO-11(DEA,1.2)	207	0.42	–	0	0.42
SAPO-11(DPA,1.2)	222	0.35	280	0.33	0.68
SAPO-11(DPA,1.6)	222	0.36	280	0.35	0.71

assigned to Si (4Si) sites.[18] This demonstrates that the silicon atoms are incorporated as large Si islands in the sample. SAPO-11(DPA,1.2) and SAPO-11(DPA,1.6) show the main peaks centered at the high-field signal (between *ca.* –100 and *ca.* –90 ppm), attributed to Si (n Al, 4-n Si, 0 < n < 4) or Si (4 Al) environments.[15,19] As a result, SAPO-11(DPA,1.2) and SAPO-11(DPA,1.6) have more acid sites than SAPO-11(DEA,1.2), in accord with the results of the NH_3-TPD (Figure 5).
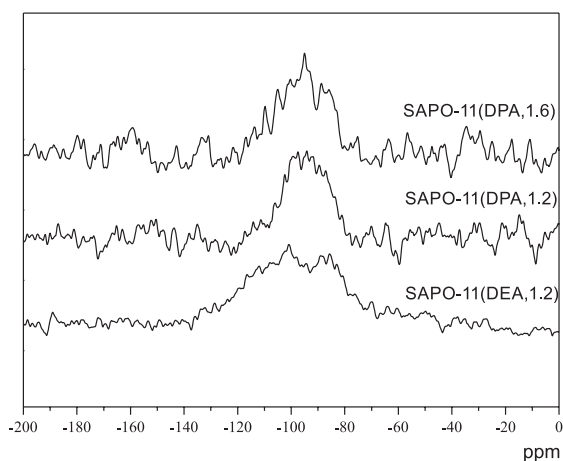
Figure 6. ²⁹Si MAS NMR spectra of SAPO-11 samples: SAPO-11(DEA,1.2), SAPO-11(DPA,1.2) and SAPO-11(DPA,1.6).

Catalytic performance

Table 3 summarizes the product distributions of the methylation of naphthalene over SAPO-11(DEA,1.2),

SAPO-11(DPA,1.2) and SAPO-11(DPA,1.6). As shown in Table 3, the main products include methylnaphthalene (MN), dimethylnaphthalene (DMN) and trimethylnaphthalene (TMN). Among all the zeolites in the present study, SAPO-11(DPA,1.2) shows the highest naphthalene conversion, 2,6-/2,7-DMN ratio and 2,6-DMN yield compared with the other SAPO-11 samples.

Table 3 shows that the naphthalene conversion over all samples decreases in the order SAPO-11(DPA,1.2) > SAPO-11(DPA,1.6) > SAPO-11(DEA,1.2), which is in accordance with the crystallinity of the three SAPO-11 samples. Generally, the high naphthalene conversion can be ascribed to the pore channels of SAPO-11 samples, which is in favor of the diffusion of the feed and the reaction products. Meanwhile, the high crystallinity corresponds to the large external surface of SAPO-11 samples, which increases the amount of pore entrances, leading to a higher probability of interaction of reagent molecules with the active centers. Table 3 and Figure 5 show that there is no coincidence between the naphthalene conversion and the acidity of SAPO-11(DEA,1.2), SAPO-11(DPA,1.2) and SAPO-11(DPA,1.6). Therefore, the difference in the naphthalene conversion is probably related to the differences in the pore structure of SAPO-11 samples. Meanwhile, it can be seen in Table 3 that the naphthalene conversion over all samples decreases with increasing reaction time. This is possibly due to the fact that some of the reactant molecules or the intermediates form in the pore channels during the synthesis process, blocking the pore channels of SAPO-11 samples and

Table 3. Comparison of catalytic performance of different SAPO-11 samples in the methylation of naphthalene

Sample	Reaction time / h	Naphthalene convension / %	Product distribution / %			2,6-/2,7-DMN	2,6-DMN yield / %
			MN	DMN	TMN		
SAPO-11(DEA,1.2)	1	48.6	52.8	38.8	8.40	1.20	4.80
	8	30.7	60.7	28.2	11.2	1.74	3.30
SAPO-11(DPA,1.2)	1	82.8	50.7	42.2	7.10	1.50	6.90
	8	56.3	58.9	32.6	8.50	1.96	5.50
SAPO-11(DPA,1.6)	1	69.4	51.6	40.9	7.50	1.35	5.80
	8	40.7	58.7	30.9	10.4	1.84	4.10

preventing further diffusion of the reactant and the product molecules,[20] thus leading to the low naphthalene conversion at longer time.

The 2,6-/2,7-DMN ratio is very important in the purification of 2,6-DMN. It is very hard to separate them when the 2,6-/2,7-DMN ratio is less than or equal to 0.7 due to the formation of the eutectic mixture of 2,6-DMN and 2,7-DMN. A higher 2,6-/2,7-DMN ratio can facilitate subsequent separation. When the 2,6-/2,7-DMN is more than 1.4, 2,6-DMN can be more easily separated from the eutectic mixture.[21-22] Table 3 also shows that the 2,6-/2,7-DMN ratio is in the order SAPO-11(DPA,1.2) > SAPO-11(DPA,1.6) > SAPO-11(DEA,1.2), which is not associated with the acidity of SAPO-11 samples. Thus, the 2,6-/2,7-DMN ratio is influenced largely by the pore structure of SAPO-11 samples. Fang *et al.*[23] calculated that the 2,6-DMN molecule is somewhat larger than 2,7-DMN, therefore, 2,6-DMN suffers more diffusion resistance than 2,7-DMN during the diffusion process. SAPO-11(DPA,1.2) exhibits broader pore size distributions than the other SAPO-11 samples do (Figure 4). The broad pore size distributions are helpful for the diffusion of 2,6-DMN, particularly the generation of the secondary mesopores over SAPO-11(DPA,1.2), which further favors the diffusion of 2,6-DMN,[24] thus finally leading to the higher 2,6-/2,7-DMN ratio.

Fraenkel *et al.*[1] reported that the naphthalene conversion over ZSM-5, mordenite and HY was of 9% at 1.33 h time on stream (TOS), 29% at 0.5 TOS and 47% at 1.33 TOS. Obviously, the naphthalene conversion over SAPO-11(DPA,1.2) is far higher than the reaction results of Fraenkel *et al.*[1] In addition, in comparison with the best results on MTW-type zeolites in the methylation of naphthalene,[25] both the naphthalene conversion and the 2,6-/2,7-DMN ratio over SAPO-11(DPA,1.2) are higher. Therefore, SAPO-11(DPA,1.2) shows high catalytic performances in the methylation of naphthalene.

Conclusion

Different SAPO-11 samples were synthesized using different templates and different template contents under hydrothermal conditions. It was found that SAPO-11 synthesized with DPA template at $n(DPA)/n(Al_2O_3) = 1.2$ shows the highest crystallinity, the highest external surface area, the broadest pore size distributions and the highest catalytic performances among all the SAPO-11 samples in this study. In comparison with other catalysts reported in the literature, it also shows higher catalytic performances for the methylation of naphthalene with methanol.

References

1. Fraenkel, D.; Cherniavsky, M.; Ittah, B.; Levy, M.; *J. Catal.* **1986**, *101*, 273.

2. Park, J. N.; Wang, J.; Lee, C. W.; Park, S. E.; *Bull. Korean Chem. Soc.* **2002**, *23*, 1011.

3. Pazzuconi, G.; Terzoni, G.; Perego, C.; Bellussi, G.; *Stud. Surf. Sci. Catal.* **2001**, *135*, 4071.

4. Bai, X. F.; Sun, K. Y.; Wu, W.; Yan, P. F.; Yan, J.; *Appl. Catal. A* **2010**, *375*, 279.

5. Lok, B. M.; Messina, C. A.; Patton, R. L.; Gajek, R. T.; Cannon, T. R.; Flanigen. E. M.; *US pat. 4440871* **1984**.

6. Song, C. M.; Feng, Y.; Ma, L. L.; *Microporous Mesoporous Mater.* **2012**, *147*, 205.

7. Prakash, A. M.; Chilukuri, S. V. V.; Bagwe, R. P.; Ashtekar, S.; Chakrabarty, D. K.; *Microporous Mater.* **1996**, *6*, 89.

8. Matsuda, T.; Kimura, T.; Herawati, E.; Kobayashi, C.; Kikuchi, E.; *Appl. Catal. A* **1996**, *136*, 19.

9. Singh, P. S.; Bandyopadhyay, R.; Rao, B. S.; *Appl. Catal. A* **1996**, *136*, 177.

10. Wang, X. X.; Wen, J.; Zhang, W.; Zhao, L. F.; Wei, W.; *Petrochem. Tech.* **2012**, *41*, 1284.

11. Wen, J.; Wang, G. Y.; Zhang, Y.; Qiu, Z. G.; Zhao, L. F.; *Petrochem. Tech.* **2012**, *39*, 487.

12. Sinha, A. K.; Sainkar, S.; Sivasanker, S.; *Microporous Mesoporous Mater.* **1999**, *31*, 321.

13. Ren, X.; Komarneni, S.; Roy, D. M.; *Zeolites* **1991**, *11*, 142.

14. Baerlocher, C.; Bennett, J. M.; Depmeier, W.; Fitch, A. N.; Jobic, H.; Koningsveld, J. M.; Meier, W. M.; Pfenninger, A.; *Molecular Sieves Science and Technology: Structures and Structure Determination*, vol. 2; Karge, H. G.; Weitkamp, J., eds; Springer: Netherlands, 1999.

15. Liu, P.; Ren, J.; Sun, Y. H.; *Catal. Commun.* **2008**, *9*, 1804.

16. Roldán, R.; Sánchez, M.; Sankar, G.; Romero-Salguero, F. J.; Jiménez-Sanchidrián, C.; *Microporous Mesoporous Mater.* **2007**, *99*, 288.

17. Ren, X. T.; Li. N.; Cao, J. Q.; Wang, Z. Y.; Liu, S. Y.; Xiang, S. H.; *Appl. Catal. A* **2006**, *298*, 144.

18. Blasco, T.; Chica, A.; Corma, A. Murphy, W. J.; Agúndez-Rodríguez, J.; Pérez-Pariente, J.; *J. Catal.* **2006**, *242*, 153.

19. Tan, J.; Liu, Z.; Bao, X.; Liu, X.; Han, X.; He, C.; Zhai, R.; *Microporous Mesoporous Mater.* **2002**, *53*, 97.

20. Lucas, N.; Bordoloi, A.; Amrute, A. P.; Kasinathan, P.; Vinu, A.; Bohringer, W.; Fletcher, J. C. Q.; Halligudi, S. B.; *Appl. Catal. A* **2009**, *352*, 74.

21. Millini, R.; Frigerio, F.; Bellussi, G.; Pazzuconi, G.; Perego, C.; Pollesel, P.; Romano, U.; *J. Catal.* **2003**, *217*, 298.

22. Mitsubishi Gas Chemical Company; *US pat. 6072098* **2000**.

23. Fang, Y. M.; Hu, H. Q.; *Catal. Commun.* **2006**, *7*, 264.

24. Wang, Q. Y.; Li, D. D.; Qi, Y.; Cao, Z. B.; Liu, Z. M.; *Ind. Catal.* **2007**, *15*, 10.

25. Wu, W.; Wu, W. G.; Kikhtyanin, O. V.; Li, L. F.; Toktarev, A. V.; Ayupov, A. B.; Khabibulin, J. F.; Echevsky, G. V.; Huang, J.; *Appl. Catal. A* **2012**, *375*, 279.